Supplemental Table S1: Melanoma protein-coding mutations in known driver genes associated with strongly positioned nucleosomes.

Gene	DNA change*	Amino acid change	Distance to nucleosome center	Nucleosome side[#]
SNX31	C>T	D275N	32	5'
ARID2	C>T	Q1313stop	3	5'
MAP2K2	**C>T**	**Q391stop**	**1**	**3'**
TP53	**C>T**	**R342stop**	**5**	**3'**
TP53	**CC>TT**	**R342stop**	**5**	**3'**
NRAS	**C>T**	**G13D**	**30**	**3'**
NRAS	**C>G**	**G12A**	**33**	**3'**
NRAS	**C>T**	**G12D**	**33**	**3'**
NRAS	**C>A**	**G12C**	**34**	**3'**
SNX31	**C>T**	**E132K**	**38**	**3'**
TACC1	**C>T**	**P407S**	**52**	**3'**
TP53	**T>G**	**V143G**	**70**	**3'**

*DNA change (i.e., mutation) is written in terms of the pyrimidine-containing DNA strand. All protein-altering mutations neighboring a strongly positioned nucleosome were included, regardless of which DNA strand the pyrimidine base was located.

[#]Mutations in which the mutated pyrimidine base was on the 3' side of the nucleosomal DNA (relative to the dyad axis) are indicated in bold.

Supplemental Figure S1

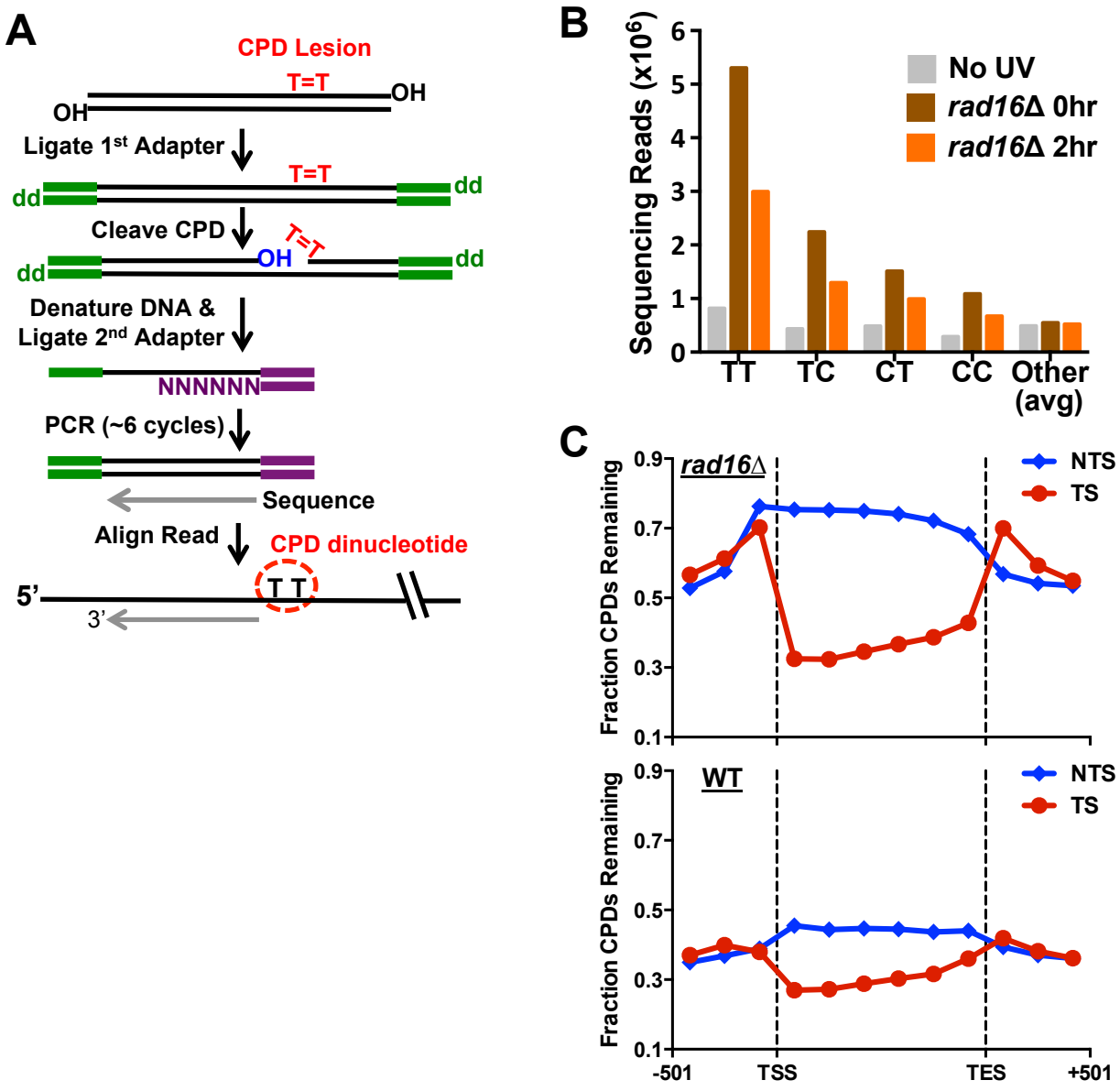

Supplemental Figure S1. (A) Schematic of CPD-seq method. DNA isolated from UV-irradiated cells is sonicated and end-repaired. First adaptor (green) is ligated and all free 3' ends are blocked by terminal transferase and dideox-ATP (ddATP). CPDs are cleaved by T4 endonuclease V and apurinic/apyrimidinic endonuclease (APE1) to generate new 3' ends. DNA is denatured and subsequently ligated to the second adaptor DNA (purple). The resulting library is purified, briefly amplified and sequenced. (B) Enrichment of dipyrimidines (i.e., TT, TC, CT, and CC) associated with CPD-seq sequencing reads in UV-treated *rad16*Δ cells. Yeast cells were UV irradiated and CPD-seq libraries were prepared immediately after UV irradiation (0hr) and following 2hr of repair. As a control, CPD-seq libraries were also prepared from unirradiated WT cells (No UV). (C) Analysis of the fraction of CPDs remaining after 2hr repair in wild-type

(WT) and *rad16*Δ mutant cells across the transcribed regions of 4971 yeast genes. Each gene was divided into 6 equally sized bins, from the transcription start site (TSS) to the transcription end site (TES), based on coordinates from (Park et al. 2014). In addition, 3 bins upstream of the TSS (i.e., -1 to -501 bp), and 3 bins downstream of the TES (+1 to +501 bp downstream of the TES) were also included. CPD counts at 2hr were divided by the initial CPD counts at 0hr to obtain the fraction of CPDs remaining for each bin. Data for *rad16*Δ (top) and WT cells (bottom) are depicted.

Supplemental Figure S2

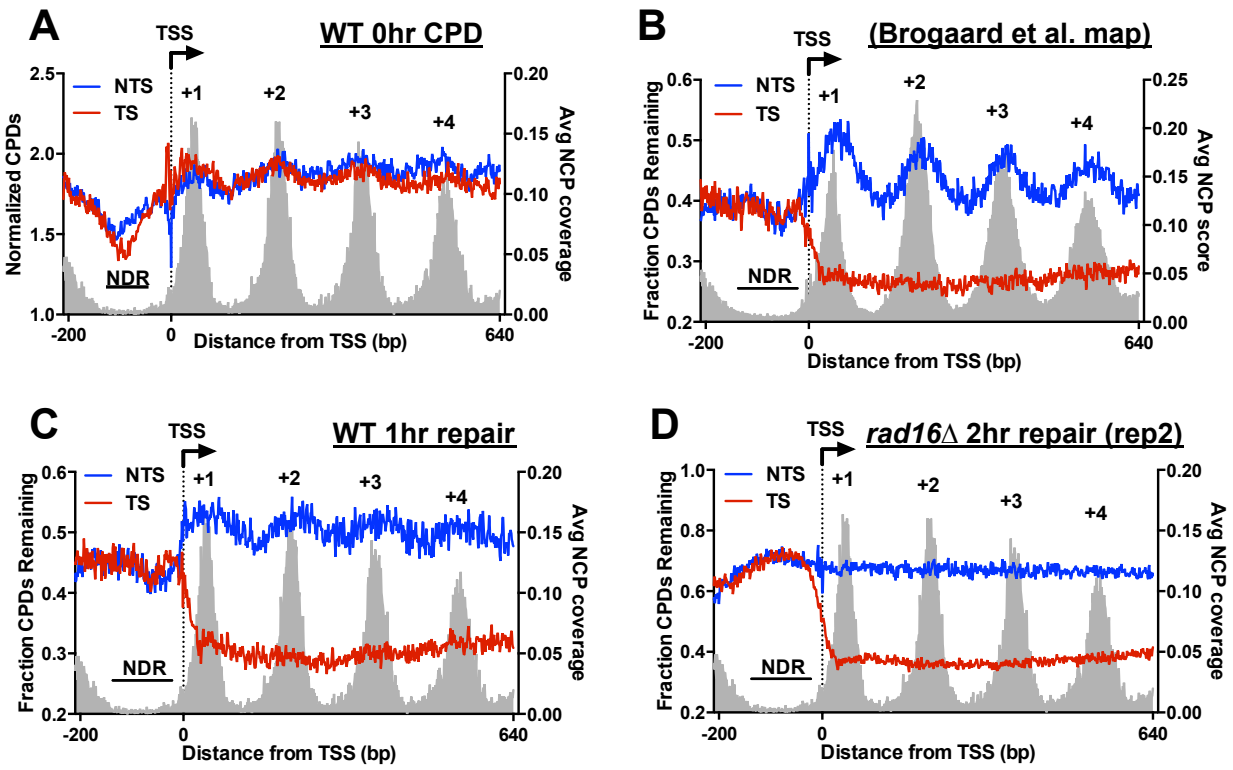

Supplemental Figure S2. (A) High resolution analysis of normalized CPD levels around the transcription start site (TSS) in wild-type (WT) cells immediately following UV irradiation (0hr). The TSS for 5205 yeast genes was aligned, and the number of CPDs associated with either the TS or NTS from 200 bp upstream to 640 nt downstream of the TSS (indicated by the dotted line/arrow) in WT cells at 0hr were counted. CPD counts were divided by the strand-specific dipyrimidine frequencies associated with each position to calculate the normalized CPD levels. The average nucleosome coverage associated with each nucleosome dyad position, derived from a published yeast MNase-seq nucleosome map (Weiner et al. 2015), was plotted in gray. NDR denotes the Nucleosome Depleted Region upstream of the TSS, and the highly phased nucleosomes downstream of the TSS are labeled as +1, +2, +3, and +4. (B) Same as part A, except CPD counts after 2hr repair were divided by the counts at 0hr at each position to analyze the fraction of remaining CPDs in the WT 2hr sample (i.e., WT-2hr / WT-0hr), using CPD-seq data from (Mao et al. 2016). The fraction of CPDs remaining (i.e., unrepaired CPDs) was compared to the nucleosome positioning score associated with each nucleosome dyad position from a chemical cleavage nucleosome map (Brogaard et al. 2012). (C) Same as part B, except CPD-seq data for the WT 1hr sample is displayed, and compared to the average nucleosome coverage associated with each nucleosome dyad position, derived from a published yeast MNase-seq nucleosome map (Weiner et al. 2015). (D) Same as part C, except the CPD-seq data following 2hr repair from a second replicate of the *rad16*Δ mutant is depicted.

Supplemental Figure S3

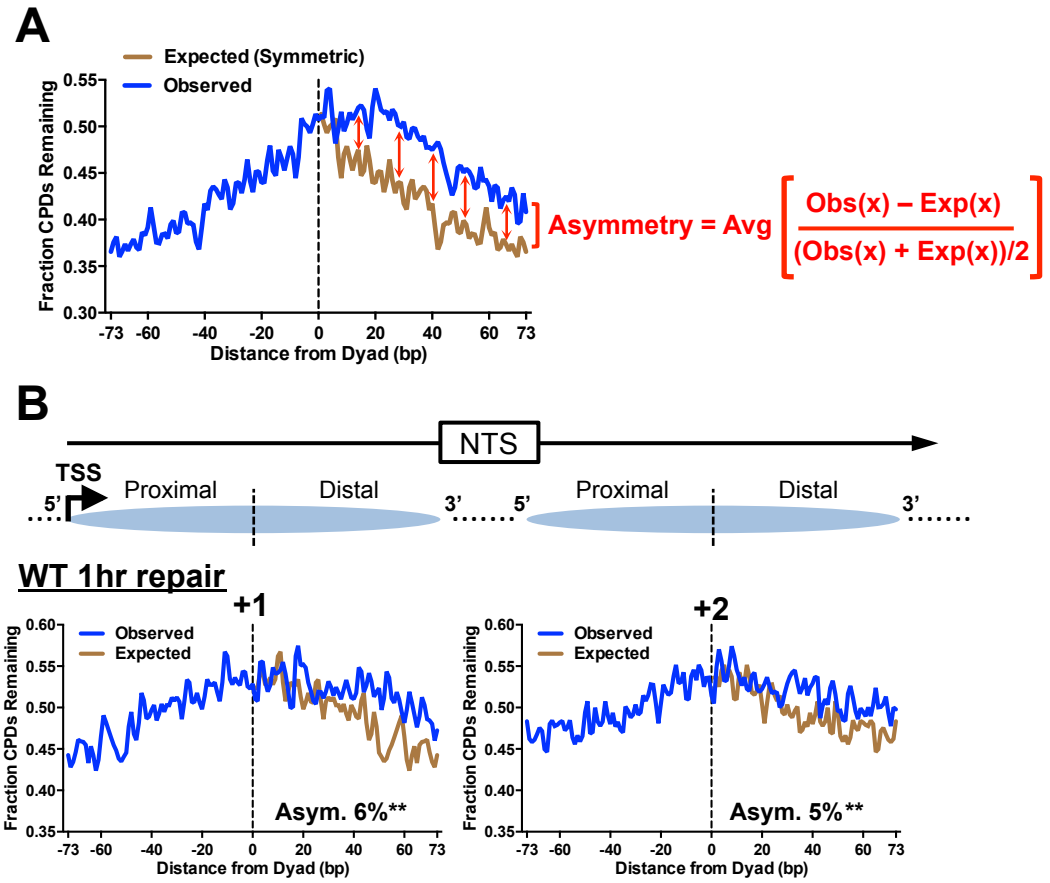

Supplemental Figure S3. (A) Schematic showing how the percent asymmetry is calculated for the CPD repair data. (B) Asymmetric removal of CPD lesions following 1hr repair in yeast intragenic nucleosomes. Top panel: diagram depicting how the NTS associated with each intragenic nucleosome (i.e., +1, +2) was consistently oriented in the 5' to 3' direction. Bottom panels: plots showing the fraction of CPDs remaining along the NTS at each position in the +1 and +2 nucleosome (i.e., -73 bp to +73 bp relative to the dyad axis) following 1hr repair in WT cells. 'Observed' plots the actual CPD repair data, while 'Expected' plots the data from the 5' side of the nucleosome on the 3' side (i.e., the expected fraction of CPDs remaining if repair was symmetric across the nucleosome dyad). The relative difference between the observed and expected curves quantifies the degree of asymmetry (Asym.) in repair, which is expressed as percent value. Nucleosome dyad positions were obtained from (Weiner et al. 2015).

Supplemental Figure S4

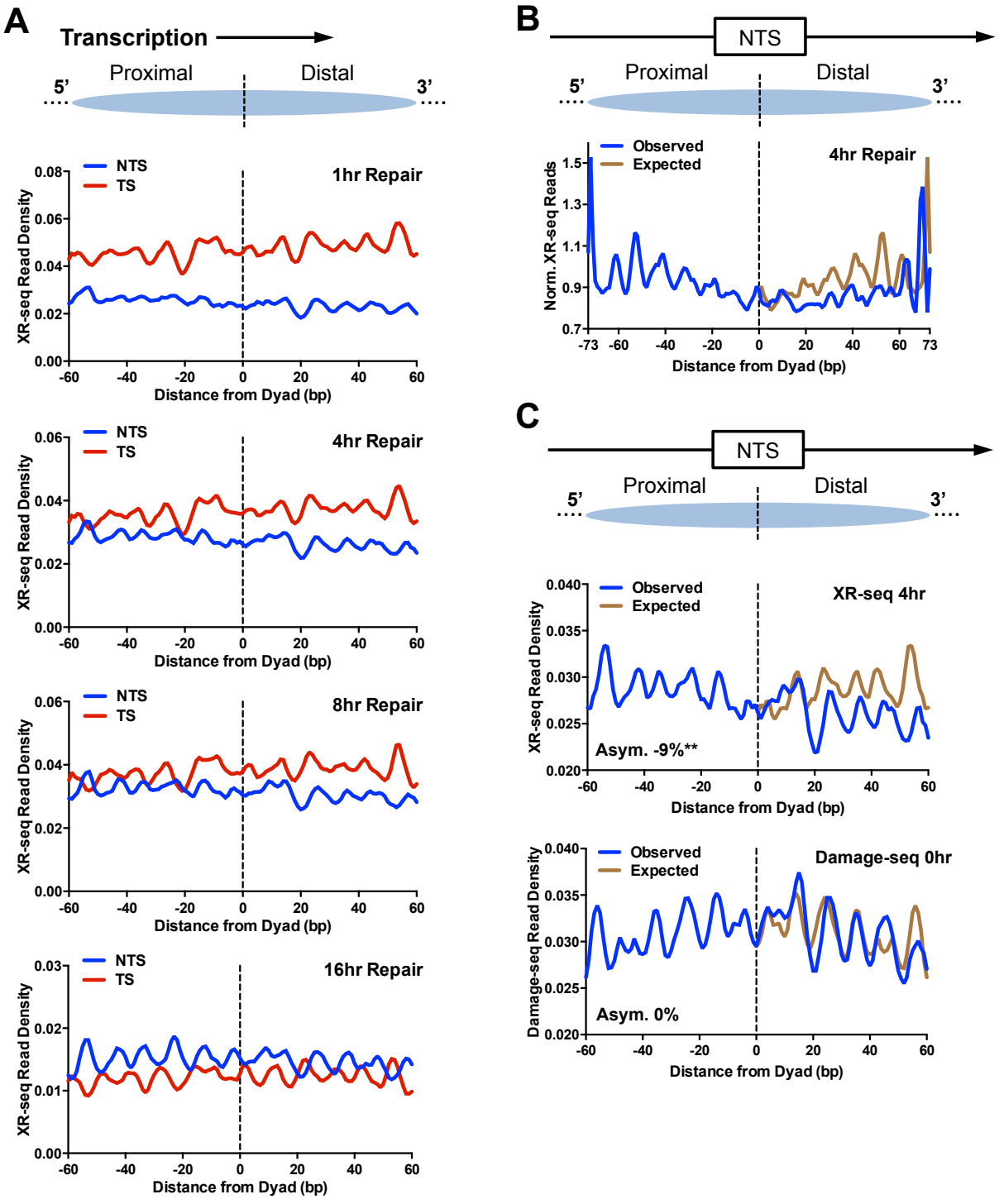

Supplemental Figure S4. (A) XR-seq read density in UV-irradiated human fibroblasts is elevated on the TS relative to the NTS at early repair time points in intragenic nucleosomes, likely due to efficient TC-NER of the TS. (B) Distribution of normalized

XR-seq read density in intragenic nucleosomes (4hr repair) from -73 to +73 nt from the nucleosome dyad axis. (C) XR-seq read density at 4hr repair (data from (Adar et al. 2016)) is asymmetric in intragenic nucleosomes (top panel), while HS-Damage-seq reads (data from (Hu et al. 2017)), measuring CPD formation immediately after irradiation (0hr), are not asymmetrically distributed. A double asterisk (**) denotes $P < 0.0001$, a single asterisk (*) denotes $P < 0.01$.

Supplemental Figure S5

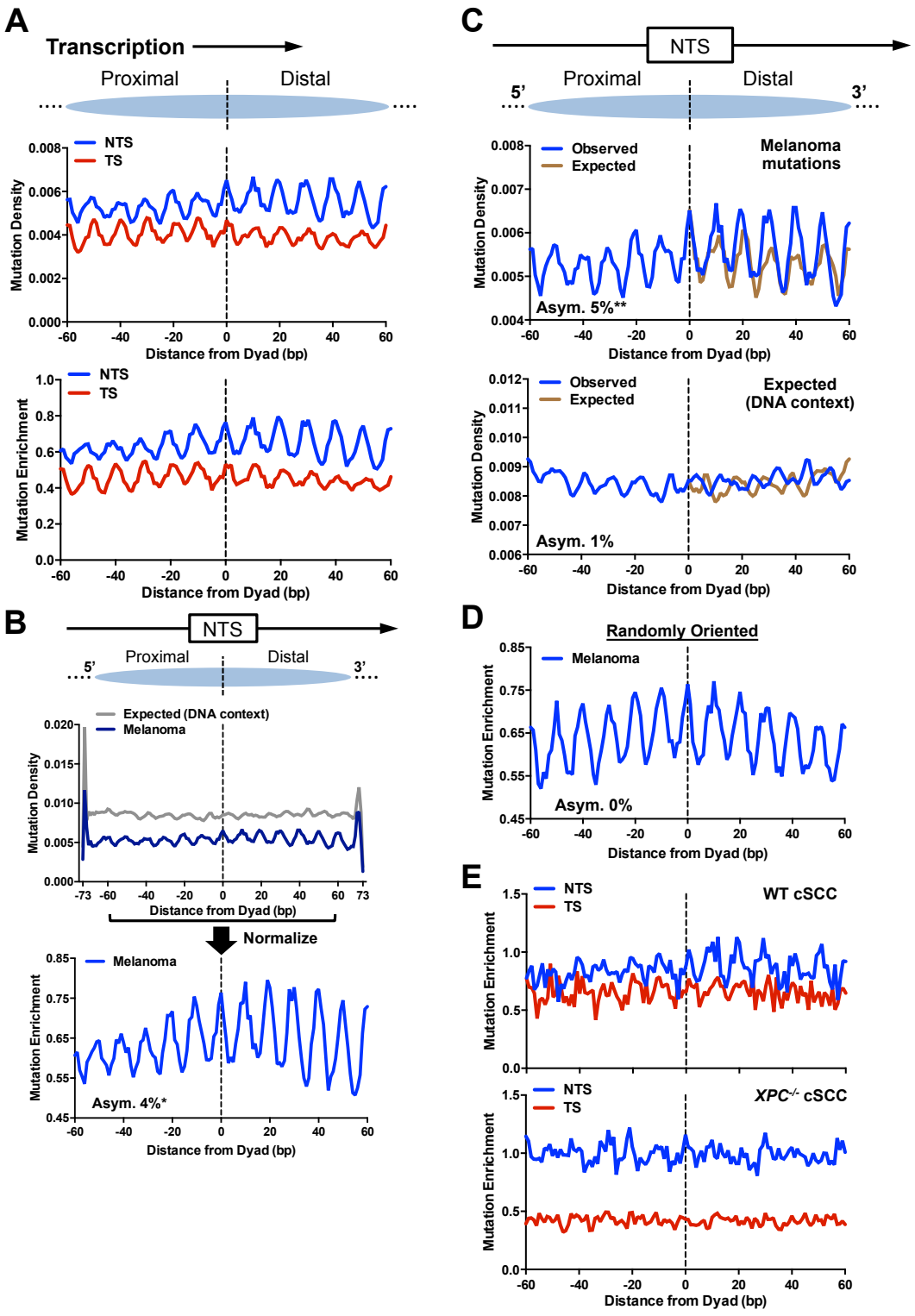

Supplemental Figure S5. (A) Somatic mutation density and enrichment in melanoma tumors are elevated on the NTS relative to the TS in intragenic nucleosomes. Mutation

enrichment was calculated by dividing the actual density of mutations along the NTS by the expected mutation density, based on the trinucleotide sequence context (see Methods). (B) Top panel: density of somatic mutations in melanoma tumors along the NTS of intragenic nucleosomes. Mutation count along the NTS was normalized by the number of pyrimidine sequences in the NTS at each position relative to the nucleosome dyad. Expected mutation density, calculated using the trinucleotide sequence context, is also plotted, and was used to calculate the mutation enrichment of melanoma mutations in intragenic nucleosomes (bottom panel). (C) Somatic mutation density in melanoma tumors is asymmetric along the NTS in intragenic nucleosomes (top panel), while expected mutation density (calculated based on the trinucleotide DNA sequence context) is not (lower panel). Actual or expected mutation density derived from melanoma tumors was plotted for the NTS at positions from -60 to +60 nt from the dyad of intragenic nucleosomes. 'Observed' plots the actual mutation (or expected mutation) density, while 'Expected' plots the data from the 5' side of the nucleosome on the 3' side. The relative difference between the observed and expected curves quantifies the degree of asymmetry (Asym.) in mutagenesis, which is expressed as percent value (see Supplemental Methods). (D) Melanoma mutation enrichment is not asymmetric when the NTS is randomly oriented (i.e., either the 5'-to-3' or 3'-to-5' orientation). (E) Mutation enrichment in cutaneous squamous cell carcinomas (cSCC) is elevated on the NTS of intragenic nucleosomes, particularly in GG-NER deficient *XPC*$^{-/-}$ tumors.

Supplemental Figure S6

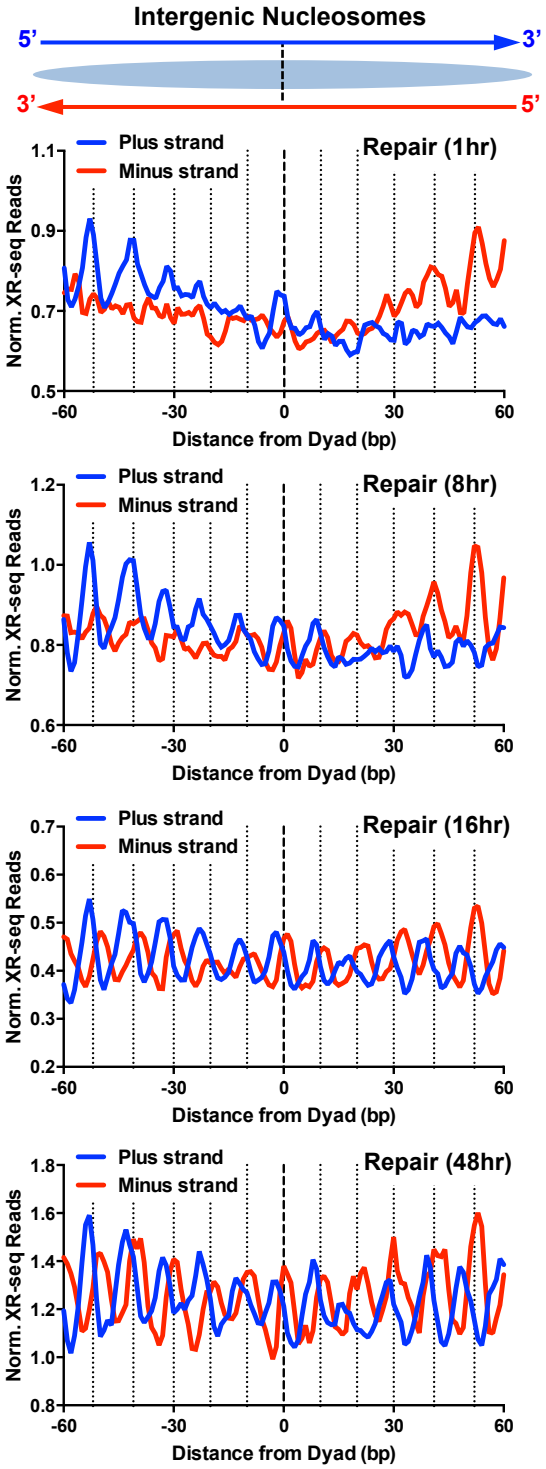

Supplemental Figure S6. Normalized XR-seq reads are elevated on the 5' side of both strands of nucleosome DNA in intergenic nucleosomes at early repair time points (e.g., 1hr and 8hr), but not later repair time points (e.g., 16hr and 48hr).